Cytoplasmic RNA in Undifferentiated Neural Stem Cells: A Potential Label-Free Raman Spectral Marker for Assessing the Undifferentiated Status

Adrian Ghita, Flavius C Pascut, M Mather, V Sottile*, I Notingher*

*corresponding author: ioan.notingher@nottingham.ac.uk, virginie.sottile@nottingham.ac.uk

Abstract:

In this study Raman micro-spectroscopy (RMS) was used to identify potential label-free spectral markers for non-invasive monitoring of the differentiation status of individual live neural stem cells (NSCs) in vitro. Label-free techniques for characterization of NCSs in-vitro are important as these cells do not exhibit surface markers, therefore labeling would render the cells unusable for regenerative medicine applications. Principal component analysis (PCA) and linear discriminant analysis (LDA) models based on Raman spectra of undifferentiated NSCs and NSC-derived glial cells enabled discrimination of NSCs with 99% sensitivity and 95% specificity. The differences between Raman spectra of NSCs and glial cells indicated that the discrimination between these cell types is based on higher concentration of nucleic acids in NSCs compared to glial cells. Comparison between Raman mapping for the 788 cm-1 and 813 cm-1 Raman bands associated with the symmetric stretching vibration of the phosphodiester bonds in nucleic acids showed that the regions with largest spectral differences are located in the cytoplasm of the NSCs and therefore can be assignment to RNAs. We propose that the observed high concentration of RNAs in NSCs is related to the repressed translation of mRNAs and large concentrations of large non-coding RNAs in the cytoplasm of undifferentiated stem cells. While this study demonstrates the potential of RMS for label-free assessment of live NSCs in vitro, further studies are required to establish the exact origin of the increased contribution of the cytoplasmic RNA.

Introduction: 750 words

Neural stem cell-based therapies are emerging approaches opening radically new strategies for the treatment of neurological diseases. Currently, neurological diseases are one of the leading causes of adult disability and it is estimated that by 2040 neurological diseases will surpass cancer as the second most common cause of death among elderly people [1]. In light of our ageing population, the development of effective therapeutic strategies for neurological disorders is of great importance. Although the potential clinical impact of stem cell therapy for neurological diseases has already been shown [2], there are still a number of challenges to overcome before it can be considered suitable for widespread, long-term use. One such challenge is the identification of appropriate cell sources and the maintenance of a stable cell phenotype during the necessary phase of in vitro expansion. Current approaches for the characterization of neural stem cells (NSCs) in vitro are experimentally intensive, often employ destructive assays rendering time-course experiments impossible, or are based on crude estimates of visual quantities which are insufficient to provide mechanistic insight into

cellular processes. In order to address fundamental questions necessary for process discovery and development of robust cell cultures for cellular therapy, new methodologies capable of quantifying key biomarkers in a non-invasive manner are urgently needed.

Conventional cell biology assays (eg. polymerase chain reaction, western blotting, etc) are invasive and are not suitable for characterizing heterogeneous cell populations since they require a large number of cells and results represent averages over entire cell populations. Fluorescence imaging can provide high-spatial resolution information for cells in vivo and in vitro, but often relies on lineage-specific surface markers that are expressed on the cell membrane [3]. However, there are numerous cases, including NSCs, where the major lineage specific markers are intracellular targets and detection requires fixation and permeabilization of cell membrane, rendering the cell unusable in a clinical environment.

Recently, Raman micro-spectroscopy (RMS) has been proposed for label-free non-invasive characterisation of stem cells and their progeny [4], [5], [6], [7], [8, 9], [10]. RMS combines the chemical specificity of Raman spectroscopy with the high spatial resolution of optical microscopy to provide detailed molecular information on cells without using labels or other invasive procedures [11]. Since water has a low Raman scattering cross-section compared to most biomolecules, Raman spectra of cells have only a minimal background signal from water. Therefore, it is possible to carry out repeated observations of viable cells maintained under physiological sterile conditions, which is difficult by other molecular vibrational techniques [8, 9], [12].

The basic hypothesis for using RMS to discriminate between cell types, including stem cells, relies on the expression of specific biomolecules by the cells at various stages of differentiation. Earlier studies reported that undifferentiated murine embryonic stem cells (mESCs) had higher concentration of mRNA compared to mESCs after 14 and 21 days of differentiation induced by removal of leukaemia inhibitory factor [4]. These biochemical differences were related with the increased translation of dormant mRNAs during differentiation of the mESCs, by similarity with maturation of oocytes [11]. Spectral differences related to nucleic acids were also reported for human ESCs (hESCs), but spectral differences were mostly associated to the smaller cytoplasm to nucleus ratio of undifferentiated cells compared to differentiated cells [7]. Comparison between different age groups of rhesus monkey mesenchymal cells derived from bone marrow also indicated a higher DNA and lower protein contribution in the Raman spectra of fetal compared to juvenile cells [13]. Spectral variations assigned to glycogen have also been reported for hESCs maintained under normal growth conditions in vitro [8], [14].

In addition to undifferentiated stem cells, RMS has also been used for non-invasive phenotypic identification of individual cells or characterization of differentiated cell cultures derived from stem cells. Comparison between Raman spectra of human bone marrow stromal cells grown in purposed-built bioreactors over 21 days in basic and osteogenic culture media showed biochemical differences related to cell differentiation and mineralisation [15]. Differences between the bone nodules formed by osteoblasts derived from mESCs and native tissues were also identified by Raman spectroscopy [16]. More recently, RMS has also been proposed for phenotypic identification of individual cardiomyocytes within highly heterogeneous cell populations as commonly obtained during in vitro differentiation of hESCs. High accuracy discrimination models based mainly on Raman bands associated to glycogen and miofibrils allowed identification of hESC-derived cardimyocytes with sensitivity >95% and specificity >95% [9]. Although currently the measurement speed is limited to only few cells per second, these initial studies are starting to progress this field towards the development of Raman-activated cell sorting for label-free enrichment and purification of cell populations with well defined phenotype [9] .

In this study we have investigated the ability of RMS to provide label-free spectral markers for non-invasive monitoring of the differentiation status of live NSCs in vitro, as well as detect spectral changes during their differentiation towards the glial phenotype. First, multivariate statistical models were developed to discriminate between undifferentiated NSCs and glial cells, then high spatial resolution Raman spectral imaging was used to correlate the observed spectral differences with intracellular molecular properties of NSCs.

Materials and Methods

Cell Culture

Cell culture reagents were purchased from Invitrogen (Paisley, UK) unless otherwise stated. Mouse neural stem cells were cultured as described elsewhere (Alcock & Sottile 2009 Cell. Res.). Briefly, cells were maintained in NSC medium prepared with DMEM/F12 and Neurobasal medium (1:1), N2, B27, Pen/Strep, bFGF (20 ng/ml) and EGF (20 ng/ml, Sigma, UK). To passage the cultures, the cells were treated with 1 ml of Accutase (Patricell Ltd, Nottingham, UK) and the sample was incubated at 37ºC for 5 minutes. After a PBS wash, the pellet was resuspended in fresh medium and transferred to a new vessel. Culture stocks were routinely split 1 in 3.

For Raman analysis, cells were seeded on Matrigel (Becton Dickinson) according to the manufacturer's instruction, to promote cell adhesion. For in vitro differentiation, NSC medium was replaced with medium containing DMEM/F12 and Neurobasal (1:1), 1% FCS, Pen/Strep. Fresh medium was added every 2 days, taking care not to disturb the monolayer. After treatment, cells were fixed with 4% ice-cold paraformaldehyde and stored at 4ºC until analysis.

Immunostaining procedure

Samples were washed in PBT (PBS + 0.1% Tween-20 (Sigma)), blocked for 1 hour in 1% blocking solution (PBT+0.1% FCS), and incubated overnight at 4ºC with an anti-GFAP antibody (Dako, Ely, UK) diluted 1/100 in 1% blocking solution. After extensive washing in PBT for 40 minutes, samples were incubated with a fluorescein-conjugated secondary antibody (Vector Labs, Peterborough, UK) for 1 hour, washed for 1 hour in PBS, and kept in PBS containing 1μg/ml Hoechst 33342 (Sigma) until imaging.

Raman micro-spectroscopy measurements

For measurements on live cells, a Raman micro-spectrometer equipped with an environmental enclosure (Solent, Segensworth, UK) was used to maintain the cells under sterile physiological conditions (culture medium, 37°C temperature, 5% CO_2). The instrument was based on an inverted microscope (IX 71,Olympus, Essex, UK) with a 60×/NA 0.90 water-immersion objective (Olympus), a 785 nm ~170 mW diode laser (before objective) (Toptica Photonics, Munich, Germany), a spectrometer equipped with a 830 lines/mm grating and cooled deep-depletion back-illuminated CCD detector (Andor Technologies, Belfast, UK) and an automated step-motor stage (Prior, Cambridge, UK). For the high spatial resolution spectral images, a second confocal Raman micro-spectrometer was used consisting of an inverted optical microscope (Ti-Eclipse, Nikon, UK) equipped with a water-immersion objective (60×/NA 1.2) (Olympus, Essex, UK), a 710 nm gaussian-beam Ti:sapphire laser (Spectra-Physics) with ~170 mW before objective, a high-precision piezo-electric XY stage (PI, Germany) connected by means of an optical fibre of 50 microns diameter to the same spectrometer. The laser beam was expanded to fill the back-aperture of the objective and thus focus the beam to a diffraction limited spot on the sample.

Both instruments were calibrated prior to each experiment using a standard tylenol sample and the spectral resolution was ~1.5cm^{-1} in the 600-1800cm^{-1} region. Purpose designed titanium cell-chambers were built, which incorporated MgF_2 coverslips (0.17 mm thick) at the bottom to enable acquisition of Raman spectra of the cells using the inverted optical configuration. For the live cells, the Raman spectrum of each individual cell represented the average of a total of 625 spectra measured at different positions inside the cell by raster-scanning the cell through the laser focus in 2 μm steps (equivalent to a grid of 25 by 25 points). The acquisition time at each position was 1 second. After the acquisition of Raman spectra was completed, the position coordinates of each cell were recorded, the cells were fixed and prepared for immunostaining (phenotypic marker and cell nucleus). The phenotypic marker of the cells was established using a wide-field fluorescence staining system integrated on the Raman microscope. The retro-positioning of each cell was achieved by using the cell coordinates (accuracy ~5 μm).

Data analysis and processing

Data preprocessing consisted of removal of spectra containing cosmic rays, background subtraction and normalization. The average of the Raman spectra measured at points outside of the cell (automatically identified using a k-means clustering analysis) represented the background spectrum (contributions from the culture medium, MgF_2 coverslip and microscope objective). The Raman spectrum representative of each cell was obtained by algebraic subtraction of the background spectrum from the average of the Raman spectra at all positions inside the cell. All Raman spectra were then normalised using the standard normal variance method.

The Raman spectra of cells were analysed by Principal Component Analysis (PCA) and linear discriminant analysis (LDA) using functions in MATLAB. Raman spectral images corresponding to selected Raman bands were obtained by calculating the area under the spectral bands after subtraction of an estimated local linear baselines and representing the integrated intensity value at each measurement position in the cell.

Results and Discussion:

Discrimination between undifferentiated neuroprogenitor and glial cells

The first aim of the study was to identify Raman spectral bands which enable discrimination between undifferentiated NSCs and NSC-derived glial cells by using non-invasive Raman spectral measurements on live cells. Fig. 1 presents bright-field, phase contrast, immuno-fluorescence images and average Raman spectra of two typical live glial cells and NSCs. When carrying out Raman spectral measurements on individual live NSCs it was found that cell motility was significant over the measurement time (~10 minutes). Therefore, to reduce errors due to cell motility, the Raman spectra of NSCs were recorded for groups of 5-6 cells (it was established that no spectral differences were detected between individual and groups of NSCs). After Raman measurements, the cells were fixed and stained to confirm the phenotype: nestin was used for undifferentiated NSCs and GFAP was used for glial cells. The phenotypic confirmation was carried out to ensure that no errors due to potential population heterogeneities were included in the Raman spectral model, as such errors can significantly reduce the phenotypic discrimination of the cells[17]. The Raman spectra in Fig. 1*E* show that the sampling method used in this study led to high signal-to-noise Raman spectra which

are representative of the entire cell analysed. The Raman spectra of both cell types consist of typical Raman bands of cellular biomolecules (nucleic acids, protein, lipids and carbohydrates) and are consistent with previous reports on other cell types [11]. Spectral differences between the glial and NSC populations can be observed in the 700-850 cm^{-1} region, which contains contributions from nucleic acids. However, to confirm these spectral differences, Fig 2 presents the average Raman spectra of 120 NSCs (CCC groups) and 40 differentiated glial cells along with the computed difference spectrum. Several Raman bands corresponding to nucleic acids can be identified in the difference spectrum which are significantly larger than the computed standard deviation. A comparison between the difference spectrum and the Raman spectra of DNA (B-conformation) and RNA in phosphate buffer saline is presented in Fig 2B. Raman bands associated to the DNA and RNA bases can be identified at 729 cm^{-1} (adenine), 782 cm^{-1} and 785 cm^{-1} (uracil, cytosine), 1578 cm^{-1} (guanine and adenine). Raman bands corresponding to the nucleic acid backbone can also be identified and used for identification of the conformation of the nucleic acids. B-conformation DNA elicits a strong band at 788 cm^{-1} and a shoulder at 835 cm^{-1} corresponding to the symmetric and asymmetric O-P-O phosphodiester stretching vibrations. For A-DNA and RNA, the symmetric vibration shifts to 813 cm^{-1} and the band corresponding to the asymmetric stretching is absent [18], [19]. In addition, a Raman band at 1098 cm^{-1} can also be identified corresponding to the PO_2^- vibrations. These results suggest that the main spectral differences between NSCs and differentiated glial cells rely mainly on a higher concentration of nucleic acids in NSCs, which is in agreement with previous Raman studies on undifferentiated ESCs [4].

A multivariate spectral model based on the principal component analysis (PCA) followed by linear discriminant analysis (LDA) was developed to enable spectral discrimination between the two cell types. The loading spectra corresponding to the first five principal components capturing 56.3% of spectral variation are showed in Figure 3. For the LDA model, only PC1, PC2, PC3, PC4, PC5 were used as other PCs did not provide discrimination, either consisted only of bands characteristic to the culture medium or were dominated by noise. The computed linear discriminant analysis loading which maximized the discrimination between the NSCs and glial cells is presented in Fig 3A and the corresponding scores in Fig 3B. The probability distribution for the LDA scores (Fig. 3*B*) shows a clear distinction between NSCs and glial cells?. To determine the true accuracy for phenotypic identification of CMs, cross-validation (CV) was used to determine the sensitivity and specificity parameters for a certain target sensitivity or specificity. The leave-one-out CV (LOOCV) showed that the LDA spectral model can discriminate between NSCs and glial cells with 99% sensitivity and 99% specificity.

Assignment of the Raman spectral differences

The computed difference spectrum in Fig 2 indicates that significant molecular changes related to nucleic acids can be identified between undifferentiated NSCs and glial cells. In particular, one can highlight the Raman band at 813 cm-1 which has been assigned to the symmetric stretching of the phosphodiester bond. However, this spectral difference could be related either to conformational changes of DNA from form B to form A or due to changes related to the RNA concentration.

A decrease in the 813 cm^{-1} band was also detected by RMS in the case of spontaneous differentiation of mESCs over a 21 days period [4]. Although the intense 813 cm^{-1} band was attributed to repressed translation of mRNAs in the embryonic stem cells followed by increased mRNA translation during the differentiation, the study did not present evidence to

discriminate between RNA and A-form DNA as only average Raman spectra over the entire cells were presented. Spectral differences related to nucleic acids were also found in undifferentiated and differentiated hESC and BMSCs [7], [13], which were attributed to a higher nucleus to cytoplasm ratio in the undifferentiated cells and associated to the increased proliferation rates compared to differentiated cells. However, neither these studies presented spatially resolved spectra to confirm that the increased signals from nucleic acids were correlated to the cell nuclei.

One of the important features of confocal RMS is that it allows the mapping of the spatial distribution of various biomolecules within individual cells which then can be compared with a higher molecular specificity than invasive techniques such as fluorescence staining. In this case, to establish whether the spectral differences were related to DNA conformational changes or to RNA concentration, Raman spectral maps for the 788 cm^{-1} and 813 cm^{-1} were measured and compared with fluorescence staining images of the same cells. Such comparisons were carried out on both NSCs and glial cells to establish whether the spectral changes corresponded to the nuclei or cytoplasm. However, Raman imaging requires raster scanning the cell through the laser focus and collection of a full spectrum at each position. Although individual Raman spectra with sufficient signal-to-noise ratio in the 700-850 cm^{-1} region can be acquired in as little as 500 ms from a given position in a cell (Supporting information Fig 1), a Raman mapping using step sizes of half the diffraction limit (500 nm) requires 20 minutes. To avoid cell movement during the Raman imaging and thus enable accurate comparison between the Raman maps and fluorescence images, the imaging was carried out on fixed NSCs and glial cells after it was confirmed that the fixation by paraformaldehyde did not affect the Raman spectra of the cells. The comparison between the Raman spectra of fixed and live cells, for both NSCs and glail cells is presented in the Supplementary information Fig S2.

Fig. 4 presents the Raman spectral maps of two typical NSCs corresponding to the 788 cm^{-1} Raman band and 813 cm^{-1} along with the corresponding phase contrast and fluorescence staining of the cell nuclei (DAPI) and cytoplasm (GFAP). Compared to the DAPI staining, the cell region of high 788cm^{-1} intensity is larger than the cell nuclei because this band consists of an overlap between the C and U ring vibration at 785 cm^{-1} and the O-P-O symmetric stretch in B-DNA. Therefore, the Raman images corresponding to the 788 cm^{-1} highlight regions rich in both DNA and RNA. However, comparison between the fluorescence images and the Raman images corresponding to the 813 cm^{-1} Raman band shows that the cell regions where these bands have high intensity correspond to the cytoplasms. To confirm the presence of the 813 cm^{-1} band in the cytoplasm of the NSCs, individual Raman spectra from locations of intense 788 cm^{-1} and 813 cm^{-1} Raman bands are also presented and compared to spectra at other positions in the cytoplasm with reduced nucleic acid contributions (spectra dominated by contributions from proteins and lipids). Based on these results, it can be concluded that the assignment of the 813 cm^{-1} band corresponds to cytoplasm RNA and not to conformational changes of the DNA. A confirmation of these findings for live NSCs but at a considerable lower spatial resolution to minimise cell motility (2 micron step size, total imaging time ~6 minutes) is presented in the Suplementary information Fig 3).

Fig 5 presents similar comparisons between Raman spectral maps of nucleic acids and fluorescence staining for two typical differentiated glial cells derived from NSCs. In this case, a very close similarity can be observed between the Raman maps corresponding to the 788 cm^{-1} band and the DAPI images of the nuclei. In addition, the Raman band corresponding to

the 813 cm^{-1} band and the selected individual Raman spectra from both cytoplasm and nuclei indicate that contrary to NSCs, contribution from nucleic acids in the glial cells can only be detected in the nucleus. Therefore, the concentration of the RNA in the cytoplasm of glial cells is considerably lower than in NSCs, becoming below the detection limit by RMS.

Although the Raman spectral maps allowed the detection of cell regions with high concentration of RNA in NSCs and not in glial cells, it may be possible that changes in the cell cytoplasm content during the differentiation of NSCs towards glial lineages can reduce the concentration of RNA below the detection level by RMS. Although an accurate evaluation is difficult, we attempted an estimation of the ratio between the cytoplasm volumes between NSCs and glial cells based on the fluorescence images and Raman maps. Assuming that the intensity of the 1450 cm^{-1} band corresponding to C-H vibrations in all biomolecules can be used as a measure of biomass, comparison between the Raman maps for this band indicated no significant differences between the heights of NSCs and glial cells (Fig 6). However, based on the fluorescence images, it can be estimated that the cytoplasm of the NSCs is approximately 2.5 times smaller than the cytoplasm of the glial cells. Based on these estimates, the increase in cytoplasmic volume for the glial cells would lead to ~2.5 fold decrease in the concentration of cytoplasmic RNA. Fig 6 B presents Raman spectra of purified RNA at various concentrations in water, acquired at similar acquisition parameters as the individual Raman spectra in Figs 4 and 5.

One possible explanation for the high Raman signal associated to the cytoplasmic RNA in NSCs is the existence of restricted translation of certain mRNAs in the undifferentiated stem cells. Early studies on lineage progenitors have reported a change in RNA content during the differentiation process. Histological analysis of embryonic brain explants has shown that neuroepithelial progenitor populations in the ependymal layer have a higher total RNA content than their mature differentiated progeny (Birge et al. 1962). In a different model, epidermal progenitors have similarly been reported to display higher RNA amounts than terminally differentiated keratinocytes (Staino-Colco at al. 1986). Interestingly, the fine dynamics of these variations over the differentiation process appears to involve a transient increase before a significant drop in RNA amounts observed in mature differentiated lineages. Further real time analysis of Raman patterns in time-course differentiation experiments will allow us to finely monitor and quantify subtle changes in nucleic acid-related peaks in a non-invasive manner, and monitor the cell status within the differentiation continuum. More recently, the importance of RNA subtypes including long non-coding RNAs and microRNAs has been highlighted in the context of cell differentiation (Dinger et al. 2008, Marcer et al. 2010, Pauli et al. 2011). Data gathered from mouse ES cells, and more recently NSCs, suggest that such non coding regulatory RNAs are dynamically regulated during the differentiation process. Further improvements in the sensitivity and discrimination potential of the Raman spectrum analysis may allow a finer characterisation of the distinct RNA components which are differentially regulated between NSCs and their progeny in live cultures.

Conclusion

RMS is an attractive technique for non-invasive characterisation of individual live cells in vitro. In this study, RMS was used to identify label-free spectral markers for label-free

monitoring the differentiation status of live neural stem cells (NSCs) in vitro. Such techniques are urgently needed for the characterisation of cell populations and assessing their differentiation status non-invasively. Principal component analysis (PCA) and linear discriminant analysis (LDA) models based on Raman spectra of undifferentiated NSCs and NSC-derived glial cells enabled discrimination of NSCs with 99% sensitivity and 95% specificity. The differences between Raman spectra of NSCs and glial cells indicated that the discrimination between these cell types is based on higher concentration of nucleic acids in NSCs compared to glial cells. Comparison between Raman mapping for the 788 cm-1 and 813 cm-1 Raman bands associated with the symmetric stretching vibration of the phosphodiester bonds in nucleic acids showed that the regions with largest spectral differences are located in the cytoplasm of the NSCs and therefore can be assigned to RNAs. These results are in agreement to previous studies on mouse embryonic stem cells. However, the lower cytoplasm to nucleus ratio of NSCs compared to the NSCs-derived glial cells cannot account for the decrease below the detection limit (factor higher than ???) in the differentiated glial cells. Therefore, we propose that the observed high concentration of RNAs in NSCs is related to the repressed translation of mRNAs and higher concentration of large non-coding RNAs in the cytoplasm of undifferentiated stem cells. While this study demonstrates the potential of RMS for label-free assessment of live NSCs in vitro, further studies are required to establish the exact origin of the increased contribution of the cytoplasmic RNA in the undifferentiated population.
This study demonstrates that the high chemical specificity of RMS represents a feasible approach to the label-free phenotypic identification of neural stem cells.

ACKNOWLEDGEMENTS:

This study was funded by grant awards from the University of Nottingham and the Biotechnology and Biological Sciences Research Council UK (BB/G010285/1). V.S. is indebted to the Anne McLaren fellowship scheme (University of Nottingham) and to the Alzheimer's Society for their support, past and present.

REFERENCES

1. Lilienfeld, D.E. and D.P. Perl, *Projected neurodegenerative disease mortality among minorities in the United States, 1990-2040.* Neuroepidemiology, 1994. **13**(4): p. 179-86.
2. Rossi, F. and E. Cattaneo, *Opinion: neural stem cell therapy for neurological diseases: dreams and reality.* Nat Rev Neurosci, 2002. **3**(5): p. 401-9.
3. Takahashi, J., et al., *Fluorescence-activated cell sorting-based purification of embryonic stem cell-derived neural precursors averts tumor formation after transplantation.* Stem Cells, 2006. **24**(3): p. 763-771.
4. Notingher, I., et al., *In situ spectral monitoring of mRNA translation in embryonic stem cells during differentiation in vitro.* Analytical Chemistry, 2004. **76**(11): p. 3185-3193.
5. Zuser, E., et al., *Confocal Raman microspectral imaging (CRMI) of murine stem cell colonies.* Analyst, 2010. **135**(12): p. 3030-3.
6. Chan, J.W., et al., *Label-Free Separation of Human Embryonic Stem Cells and Their Cardiac Derivatives Using Raman Spectroscopy.* Analytical Chemistry, 2009. **81**(4): p. 1324-1331.

7. Schulze, H.G., et al., *Assessing differentiation status of human embryonic stem cells noninvasively using Raman microspectroscopy.* Analytical Chemistry, 2010. **82**(12): p. 5020-7.
8. Turner, R.F.B., et al., *Evidence of marked glycogen variations in the characteristic Raman signatures of human embryonic stem cells.* Journal of Raman Spectroscopy, 2011. **42**(5): p. 1135-1141.
9. Pascut, F.C., et al., *Noninvasive detection and imaging of molecular markers in live cardiomyocytes derived from human embryonic stem cells.* Biophys J, 2011. **100**(1): p. 251-9.
10. Notingher, I., et al., *Noninvasive Detection and Imaging of Molecular Markers in Live Cardiomyocytes Derived from Human Embryonic Stem Cells.* Biophysical Journal, 2011. **100**(1): p. 251-259.
11. Notingher, I. and L.L. Hench, *Raman microspectroscopy: a noninvasive tool for studies of individual living cells in vitro.* Expert Review of Medical Devices, 2006. **3**(2): p. 215-234.
12. Notingher, I., et al., *Non-invasive time-course imaging of apoptotic cells by confocal Raman micro-spectroscopy.* Journal of Raman Spectroscopy, 2011. **42**(3): p. 251-258.
13. Tarantal, A.F., et al., *Growth, differentiation, and biochemical signatures of rhesus monkey mesenchymal stem cells.* Stem Cells and Development, 2008. **17**(1): p. 185-198.
14. Konorov, S.O., et al., *Absolute quantification of intracellular glycogen content in human embryonic stem cells with Raman microspectroscopy.* Analytical Chemistry, 2011. **83**(16): p. 6254-8.
15. Pully, V.V., et al., *Microbioreactors for Raman microscopy of stromal cell differentiation.* Analytical Chemistry, 2010. **82**(5): p. 1844-50.
16. Gentleman, E., et al., *Comparative materials differences revealed in engineered bone as a function of cell-specific differentiation.* Nat Mater, 2009. **8**(9): p. 763-70.
17. Chan, J.W., et al., *Micro-Raman spectroscopy detects individual neoplastic and normal hematopoietic cells.* Biophys J, 2006. **90**(2): p. 648-56.
18. Brown, K.G., et al., *Conformationally dependent low-frequency motions of proteins by laser Raman spectroscopy.* Proc Natl Acad Sci U S A, 1972. **69**(6): p. 1467-9.
19. Benevides, J.M. and G.J. Thomas, Jr., *Characterization of DNA structures by Raman spectroscopy: high-salt and low-salt forms of double helical poly(dG-dC) in H2O and D2O solutions and application to B, Z and A-DNA.* Nucleic Acids Res, 1983. **11**(16): p. 5747-61.

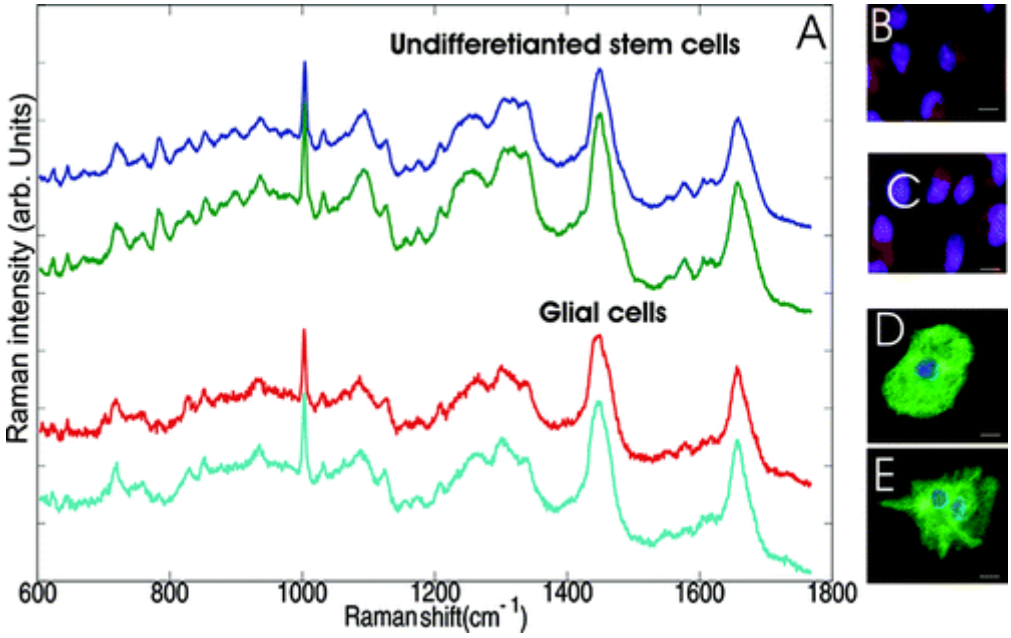

Figure1: typical bright field images of undifferentiated stem cells (A), (B). fluorescence images of undifferentiated stem cells stained for Nestin (F), (G). typical phase contrast images of glial cells (C), (D) (H). fluorescence images of glial cells stained for GFAP (H) (I). Computed average Raman spectra of live cells for undifferentiated cells and glial cells (E)

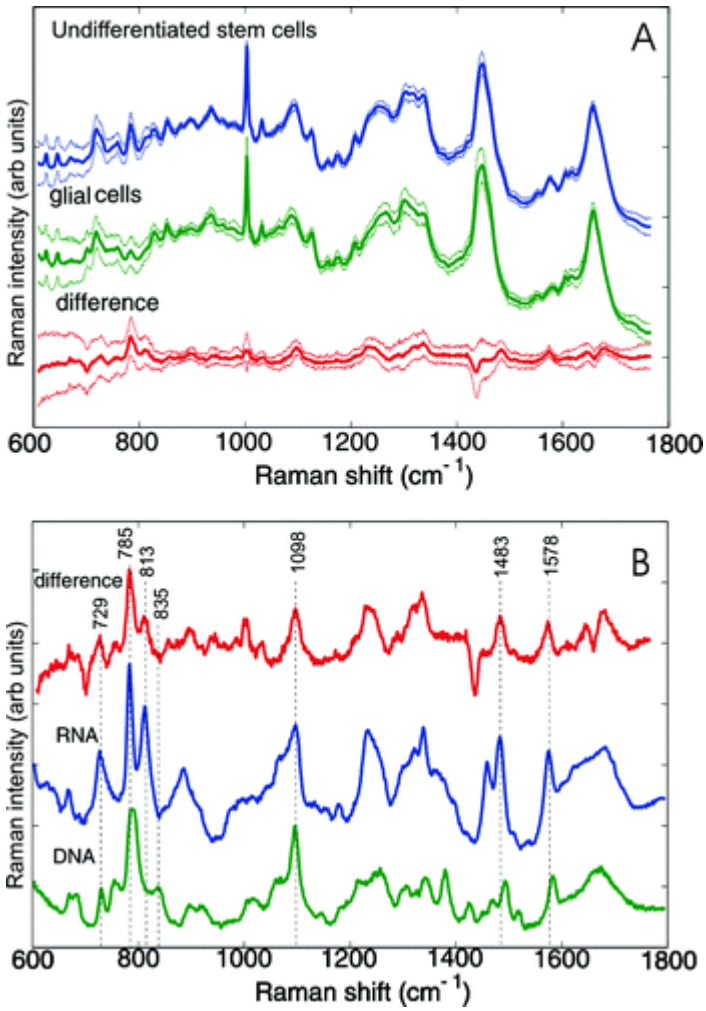

Figure 2: Average Raman spectra of undifferentiated neural stem cells and glial cells, and their computed difference, side lines represent the standard deviation calculated at each wavenumber(A). Comparison between the computed difference and nucleic acids (RNA- green spectrum, DNA-red spectrum) (B)

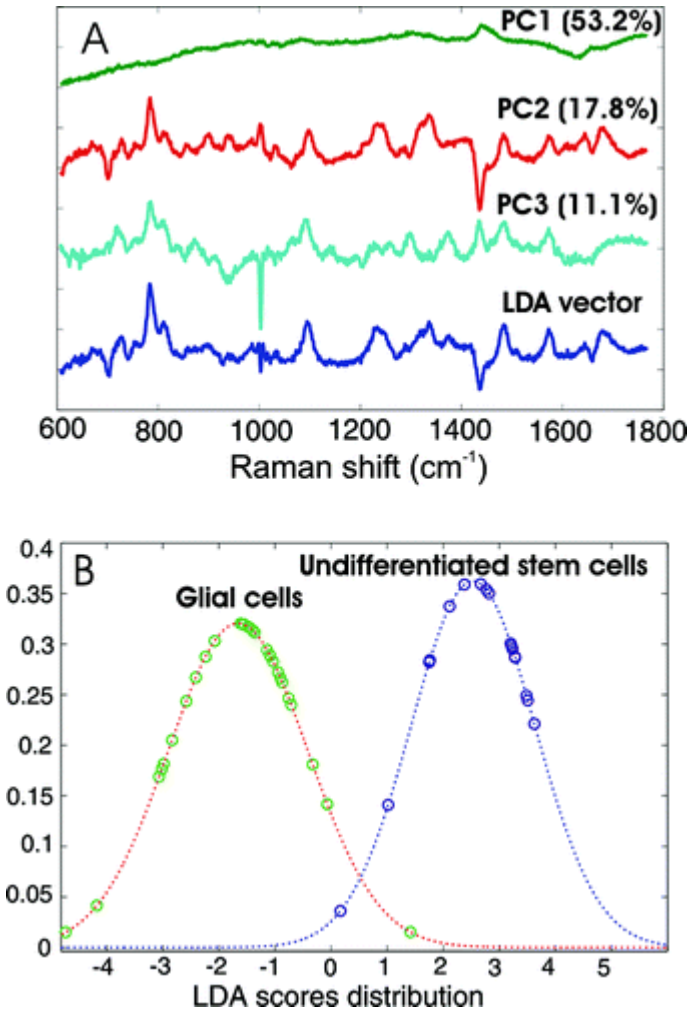

Figure 3: First five PC loadings spectra in the PCA of Raman spectra of undifferentiated NSCs and glial cells. The variance captured by each PC is shown in brackets. LDA discrimination vector (yelow) (A). Distribution of LDA scores for undifferentiated stem cells (purple dots) and glial cells (green dots) (B)

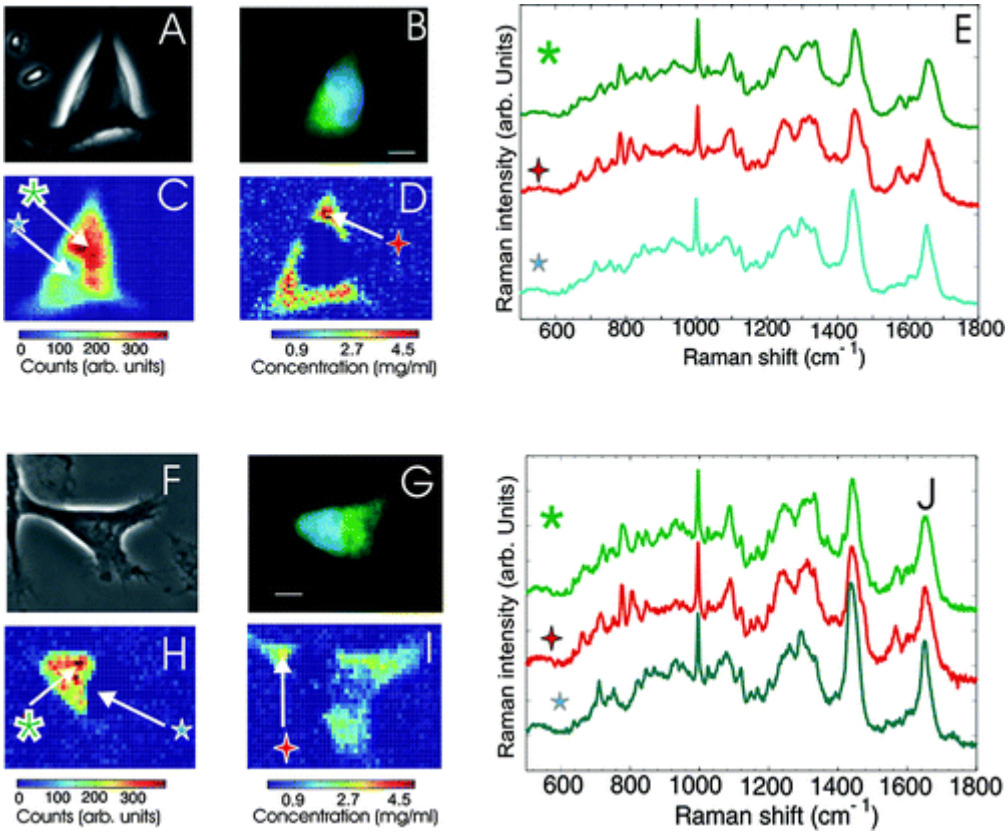

Figure 4: typical phase contrast images of fixed undifferentiated stem cells (A),(F); typical fluorescence images of the same cells (B), (G); peak area images at 788 cm-1 (C), (H); peak area images at 813 cm-1 (D), (I); individual Raman spectra taken for DNA region (green star), RNA region (red star) and phospholipids (blue star) (E), (J)

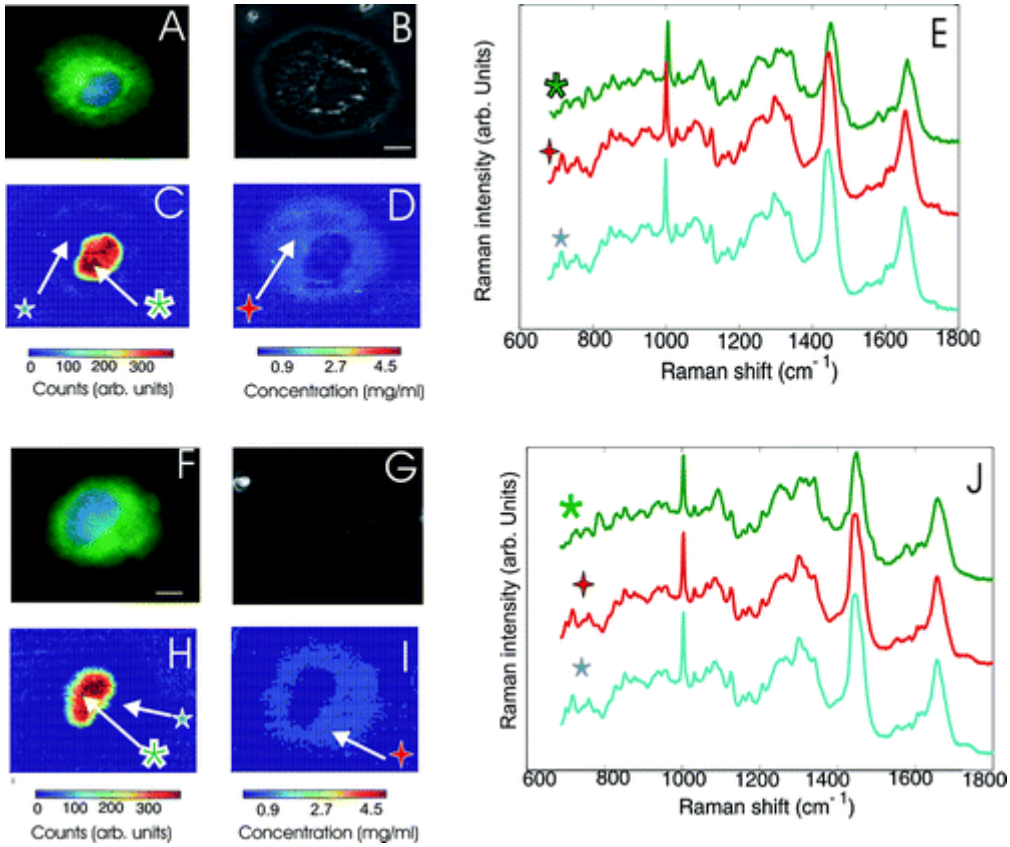

Figure 5: typical phase contrast images of fixed glial cells (A),(F); typical fluorescence images of the same cells (B), (G); peak area images at 788 cm-1 (C), (H); peak area images at 813 cm-1 (D), (I); individual Raman spectra taken for DNA region (green star), RNA region (red star) and phospholipids (blue star) (E), (J)

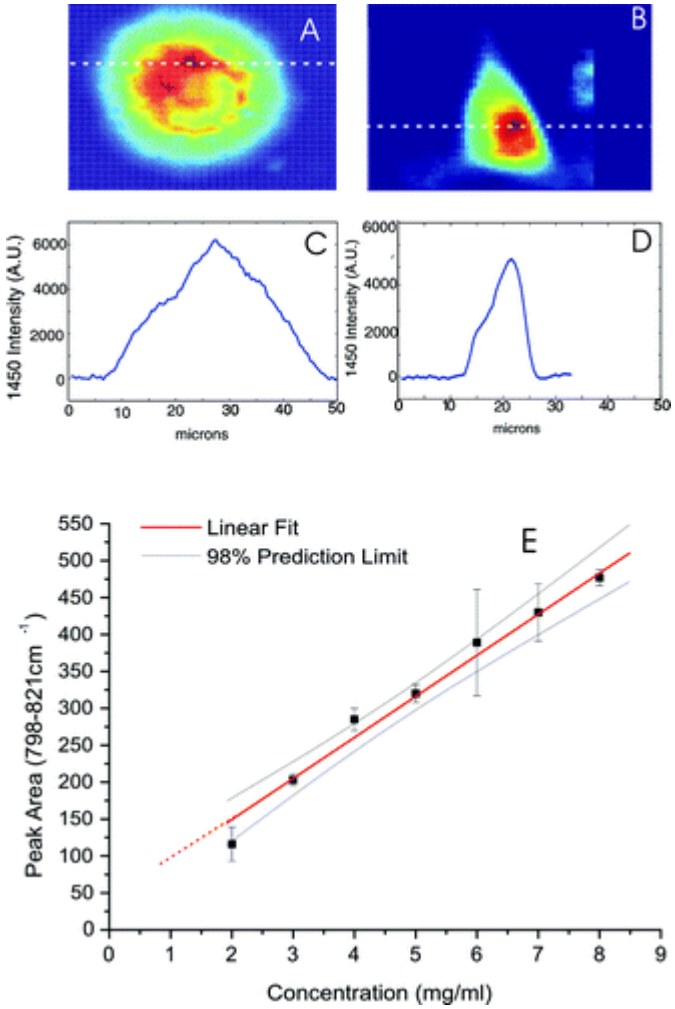

Figure 6 peak area images at 1450 cm-1 for glia, undifferentiated cell respectively (A), (C). line profile taken from 1450 cm-1 images for glia, undifferentiated cell respectively (B),(D).